Astron. Astrophys. 270, 177–188 (1993)

ASTRONOMY AND ASTROPHYSICS

A series of VLBI images of SS 433 during the outbursts in May/June 1987

R.C. Vermeulen[1,⋆], R.T. Schilizzi[2], R.E. Spencer[3], J.D. Romney[4], and I. Fejes[5]

[1] Leiden Observatory, P.O. Box 9513, NL-2300 RA, Leiden, The Netherlands
[2] Netherlands Foundation for Research in Astronomy, P.O. Box 2, NL-7990 AA, Dwingeloo, The Netherlands
[3] Nuffield Radio Astronomy Laboratories, Jodrell Bank, Macclesfield, Cheshire, SK11 9DL, United Kingdom
[4] National Radio Astronomy Observatory, Edgemont Road, Charlottesville, VA 22901, USA
[5] Satellite Geodetic Observatory, Penc, H-1373, Budapest, Pf 546, Hungary

Received January 23, accepted November 18, 1992

Abstract. Six high quality very long baseline interferometry (VLBI) images of SS 433 at a resolution of 10 milliarcseconds have been obtained at two-day intervals. The data are in excellent agreement with optically derived parameters of the so-called kinematic model: nodding motion, light travel-time effects, and Doppler boosting are clearly detected in the VLBI images. We measure a distance to SS 433 of 4.85 ± 0.2 kpc. Most 5 GHz radio emission originates on size scales larger than $\sim 10^{13}$ m. The images are consistent with intrinsically symmetric emission from the twin jets. Radio flares originate in or near the core of the system as well as in knots further away in the jets. We confirm earlier observations that such knots brighten while moving out to ∼ 250 AU from the binary system, and that they fade rapidly at larger distances. We also discuss evidence for continuous ejection in the jets of SS 433 and show that ∼ 100 AU wing-like protrusions from the core are consistently present in all 6-cm images of SS 433. Material ejected from SS 433 may brighten and fade twice.

Key words: SS 433 – radio continuum: stars – jets – stars: flare – VLBI – stars: distances

1. Introduction

In May/June 1987, a multi-wavelength monitoring campaign was carried out on SS 433. Here, we present a sequence of six very long baseline interferometry (VLBI) images. Reports on other aspects of the 1987 campaign are given in this issue of Astronomy and Astrophysics by Aslanov et al. (1993), Vermeulen et al. (1993a), and Vermeulen et al. (1993b). Complementary X-ray observations were published by Kawai et al. (1989).

Send offprint requests to: R.C. Vermeulen

⋆ Present address: Owens Valley Radio Observatory, California Institute of Technology, Pasadena, California 91125, USA

An overview of the unusual nature of SS 433 was given by Margon (1984). The unique double set of moving Doppler shifted emission lines in its optical spectrum is widely accepted as evidence for the presence of a pair of anti-parallel jets, in which matter is ejected at 0.26 c. The jets are observed to precess with a period somewhat under half a year, often referred to as the 164-day motion. This is described by the so-called kinematic model, proposed by Abell & Margon (1979), and independently by Milgrom (1979). The kinematic model has been refined to describe various complications; the most important being a ∼6.3 day nodding motion superimposed on the precession. An analysis with best-fit parameters based on almost a decade of data is given by Margon & Anderson (1989).

The presence of precessing jets is strongly supported by radio images with a resolution ranging from 4.4 arcmin (Downes et al. 1981) down to 10 milliarcsec (e.g. Vermeulen et al. 1987). It is generally accepted that ballistically moving matter is successively ejected at different angles by a precessing "gun barrel" which is tied to an unknown acceleration and collimation mechanism. This results in a curved emission trace, which is visible on scales below ∼1 arcsec, in images made with the VLA (e.g. Hjellming & Johnston 1985), with MERLIN (e.g. Spencer 1984), and with VLBI (e.g. Romney et al. 1987). Such images complement the radial velocity information in the optical emission lines, and indeed, early VLA images (Hjellming & Johnston 1981a), helped to resolve a degeneracy in the parameters of the kinematic model. Here, we present the first series of VLBI images in which the kinematic model can not only be verified from the curvature of the emission, but also from the unambiguously observed proper motion of individual features. Spencer (1984) analysed MERLIN images in the same way. We will extensively discuss component identification, and distance and velocity determinations, in Sect. 3.

On scales below ∼0.5 arcsec the radio jets are dominated by discrete features. Their evolution as seen in MERLIN images was described by Spencer (1984), while Hjellming & Johnston

Table 1. The observing log. A tick mark indicates the successful participation on the indicated day of the VLBI station listed at the top of the column. For each station, we list the antenna diameter, the typical system temperature, the sensitivity, and the frequency standard used (R=Rubidium oscillator, H=Hydrogen maser)

		Effelsberg Germany	Jodrell Bank UK	Onsala Sweden	Medicina Italy	Westerbork Neth.	Greenbank USA
Diameter (m)		100	25	25	32	93[a]	42
T_{sys} (K)		65	125	80	70	70	40
Sensitivity (K/Jy)		1.4	0.076	0.06	0.17	0.35	0.50
Frequency standard		H	R	H	H	H	H
Image	JD−2440000						
1	6938.6	√	√	√	√	√	√
2	6940.6	√	√	√	√	√	—
3	6942.6	√	√	√	√	√	—
4	6944.6	√	√	√	√	√	—
5	6946.6	√	√	√	√	√	√
6	6948.6	√	√	√	√	√	√

[a] Equivalent diameter of 14 separate 25 m dishes

(1988) recently presented an expanding plasmon model to fit the extended emission of the VLA images. Numerous discrete features were also found in the many observations on VLBI scales made since 1979 (see Vermeulen et al. 1987; Romney et al. 1987, and references therein). Most of the radio emission arises on scales of $\sim 10^{13}$ m ($\sim$ 15 milliarcsec) and larger, but Walker et al. (1981) reported a 30 mJy compact ($< 10^{12}$ m) core component at 10 GHz. All previously published maps are consistent with the core being the brightest radio feature of SS 433. Blobs are often, but not always, ejected symmetrically in the two jets. Their occurrence can often be associated with flares in the total flux density of SS 433, but this is again not invariably true. There may be some fainter more continuous emission in the jets, and there is some evidence for occasional deviations from the kinematic model (see Romney et al. 1987).

Romney et al. (1987) and Schilizzi et al. (1984) have presented early attempts to follow the evolution of individual features on VLBI scales. A series of six maps with higher sensitivity, made in 1985 at two-day intervals, was discussed by Vermeulen et al. (1987, herein after Paper I). The structure in those maps is consistent with a number of individual unresolved ($\leq 10^{13}$ m) blobs, which all display a proper motion in accordance with the kinematic model for a distance of $\sim$5 kpc. They brighten at a substantial distance from the core ($\sim 4 \times 10^{13}$ m), and then fade rapidly. Many other published VLBI maps have features that support the existence of a brightening zone at a more or less fixed distance from the centre, as was pointed out by Fejes et al. (1988). Several explanations are possible. It was pointed out in Paper I that brightening could occur when a new blob overtakes the bow-shock of its predecessor. This mechanism leads to a well defined brightening distance without requiring special conditions in the medium around SS 433.

We present a new sequence of six VLBI images of SS 433 at 5 GHz with a resolution of 10 milliarcsec (mas); their dynamic range is the highest ever achieved for SS 433 at this resolution. We also discuss more limited data at even higher resolution. The set of six observations to be discussed here is in some respects a counterpart to the 1985 set presented in Paper I. The earlier measurements were obtained when the jets of SS 433 were almost in the plane of the sky, but during the 1987 series there was a substantial radial velocity component, which leads to Doppler boosting and light travel-time differences between the two jets. The angle between the jets and the line of sight had reached its minimum in the $\sim$162.50 day precession cycle at JD 2446919.3 (Margon & Anderson 1989). During the earlier observations, SS 433 was quiescent, while the behaviour to be discussed here is connected to radio flaring, which was observed in simultaneous monitoring at many frequencies (Vermeulen et al. 1993a). The sensitivity of our data is twice as high as that of the data in Paper I.

The observations, the data reduction and the image fidelity achieved are discussed in Sect. 2. Section 3 is devoted to an analysis of the six images. We first explain our method to align them. The images are described in terms of a complex core component and additional separate knots. In Sect. 4, the evolution of these two components is analysed and related to features seen in earlier maps and to the radio flaring observed by Vermeulen et al. (1993a). Section 5, finally, summarises the results.

2. Observations and data reduction

2.1. Overview of the observations

SS 433 was observed six times at two-day intervals in May/June 1987, using five stations of the European VLBI Network (EVN), at a frequency of 4990 MHz. MERLIN observations, obtained simultaneously, are being prepared for publication in another paper, which will also draw on more recent data, and will focus on the evolution of the jets on larger scales. During three of the six EVN measurement epochs, the Green Bank 43 m telescope

joined in the VLBI observations. Table 1 shows the available data at each observing epoch, and also summarises the specifications of the participating telescopes. Henceforth, we will refer to the six observations by image or day number; the Julian Date of the middle of each observation is listed in Table 1 (Image 1 = Day 1 = JD 2446938.6, etc.). The percentage of data lost due to mishaps of various kinds was remarkably low, which is a tribute to the many persons involved in operating the array.

We used the Mark III recording system (Rogers et al. 1983) in its most sensitive Mode A: all VLBI stations recorded a 56 MHz band in left-circular polarisation. This choice implied that continuous recording was impossible; for each 11-hour synthesis, we obtained 219 minutes of data on SS 433, mostly in stretches of 13 minutes, as well as a few scans on a calibrator, PKS 2121+053. Simulations were performed before the experiment to determine how the (u, v)-plane coverage could be optimised for imaging the structure in the (largely east-west) jets of SS 433. We believe that we have succeeded in designing the experiment in such a way that the intermittent data recording has not been the limiting factor in the image quality achieved.

2.2. Data reduction

All data were correlated at the Mark III processor operated by the Max-Planck-Institut für Radioastronomie in Bonn, Germany. The coherent integration time was limited to 2 minutes, in view of phase noise losses due to the use of a rubidium oscillator in Jodrell Bank. It would also not have been prudent to use the maximum possible 13 minute integration time, since the outer compact features in the images lead to rapid variations in the visibility function on the scales sampled by the EVN. SS 433 was always detected on all EVN baselines, but on the transatlantic baselines (to Green Bank), fringes were often not detected above the $6\,\sigma$ level. The shortest (u, v)-distance on the transatlantic baselines is $\sim$ 3.5 times greater than the longest (u, v)-distance within the EVN. Hence, the Green Bank baselines were not used for hybrid mapping.

The same a priori calibration procedures were applied as described in Paper I, based on telescope gain curves as a function of elevation and system noise temperatures which were typically measured every hour. We then successfully determined time-dependent corrections per telescope, by requiring internal consistency in the calibrator dataset. As also described in Paper I, a careful appraisal was made of the influence of questionable data sections on the final images. No features discussed here were found to depend on the retention or removal of dubious data sections.

Hybrid maps were made using, independently, both the NRAO AIPS package (programmes ASCAL, MX), and the Jodrell Bank OLAF package (programme MAP). All features to be discussed were found in both sets of independently produced images. However, the dynamic range of the final images was improved by doing the initial iterations in OLAF, and the final ones in AIPS. The easy interactive multi-windowing capabilities of OLAF facilitate a careful control of the model used for phase self-calibration, while the AIPS software seems to be superior in solving the fourier transform and deconvolution problem when the final image is made from well-calibrated data. The phase self-calibration was started using an unresolved point source model; a very poor approximation to many of the images, which show knots in the jets containing a major fraction of the total flux density. Hence, it was important to use many iterations, expanding the source model only a little each time.

Figure 1 shows the final EVN images, all at the same angular scale, which is indicated on the frame. We display the images with a constant vertical offset between their adopted centres; the issue of aligning the images is treated in Sect. 3.1. The (u, v)-plane coverage was similar enough at each epoch to allow the same restoring beam to be used for each image. Identical absolute contour levels were chosen for all images, to enable the reader to follow the flux density evolution. Figure 2 shows the brightness profile of the jets of SS 433. The profiles are crosscuts through the images in Fig. 1, along the curved kinematic model prediction.

2.3. Image fidelity

One of the major uncertainties in producing the images lies in the flaring that took place during the measurements. The multi-frequency radio monitoring discussed by Vermeulen et al. (1993a) shows that one may expect differences of up to 20 percent in the total flux density between the start and the end of a synthesis. Such differences might introduce spurious structure. Amplitude self-calibration was therefore confined to one cycle at the end of the hybrid mapping iterations, and even then we only allowed a recalibration of the sensitivity of each telescope by a time-independent factor, a procedure little affected by the slopes in the visibility amplitudes due to flaring.

It is immediately obvious from the six independent images, that the flares did not take place in a single, unresolved component (e.g. the core). It is therefore impossible to perform a model-independent recalibration with time of the visibility amplitudes, by using the total flux density evolution measured by Vermeulen et al. (1993a). A hybrid mapping scheme is being developed by Vermeulen & Rugers (in preparation) that allows an iterative determination of the time-dependent models needed to (self-)calibrate the visibility data. This scheme is also intended to handle the effects of the motion of features in the jets of SS 433 (0.26 c at 5 kpc implies a proper moti on of $\sim$ 0.5 beamwidth in one synthesis). For the images presented here we have not yet been able to use this algorithm, but the work of Vermeulen and Rugers has already yielded valuable information on the image fidelity.

Partly as a result of the source variability over the course of each measurement, the noise level achieved is 1.5 mJy, whereas the expected (thermal noise) level is 0.3 mJy. We are confident that the overall source morphology shown in Fig. 1 is essentially correct. That is, we believe that the images do not show features above the achieved noise level in locations where there should be no emission, and we also believe that we have not missed any real component of SS 433 above that noise level. However, there is some uncertainty in distributing changes in the total flux

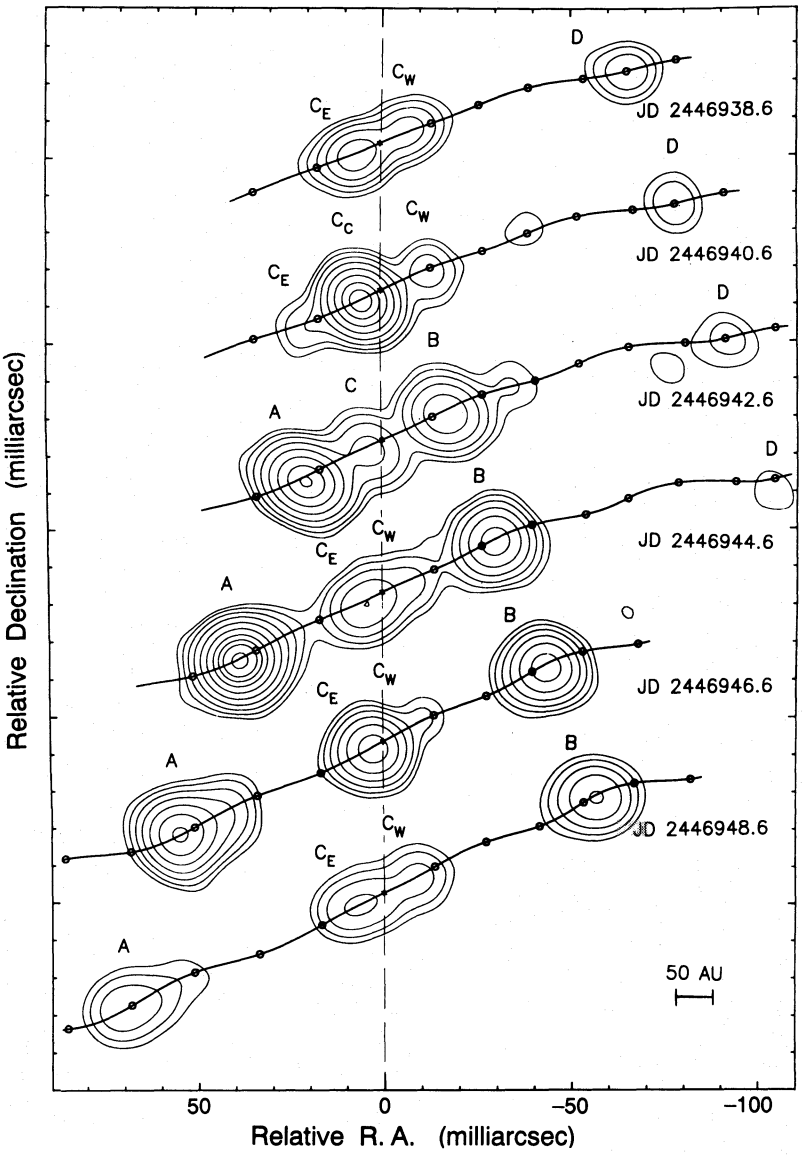

Fig. 1. European VLBI Network images of SS 433, observed at two-day intervals. The same absolute contour levels are displayed for all six images: 2, 4, 8, 16, 32, 60, 100, 140, 180, 240 mJy/beam. The same circular restoring beam was used for all images (10 mas or ~50 AU FWHM, shown in the lower right-hand corner). The images are displayed with equal vertical offsets between the adopted centres. The relative alignment is explained in Sect. 3.1. Our preferred choice for the location of the binary system is shown by the vertical dashed line, and is explained in Sect 3.2 . The locus of emission predicted by the kinematic model, including nodding motion, is drawn through each image. Markers indicate ejection age intervals of 2 days along that locus. Labels refer to individual features which are discussed in the text

density over the different features in the images, even though we are very confident about the reality of these features. In Images 3, 4, and 5, where the flux density evolves most rapidly, the relative flux density of all features is uncertain by up to $\sim$ 15 percent. More strictly speaking, this is the relative uncertainty of the the flux density contained in any particular synthesised beam area with respect to another, independent area. In addition, uncertainties in the flux density calibration of the array lead to a $\sim$ 10 percent margin in the absolute flux scale of the images. This affects only the global level of the images.

Each independent image could have been affected differently by the rising and falling flux density of the components of SS 433, and we regard the consistent evolution seen from image to image as an important validation of their correctness. A consistent evolution was also found between images which were made separately from the first and second half of each dataset. The images obtained in these tests have inferior resolution and dynamic range, and are not shown. In our further discussion, we will concentrate on the global morphological evolution of the images, and on the gross changes in flux density, which are firmly established.

3. Analysis

3.1. Alignment of the images

In any *single* VLBI image one does not know a priori where the core is located, i.e. which radio knot is related to the SS 433 binary system. In earlier work, the brightest component was generally assumed to be the core, and this registration usually gave a good agreement between the kinematic model and the radio corkscrews (Vermeulen et al. 1987; Romney et al. 1987). For the present *series* of VLBI images no indirect argument is needed for a global registration of the core. Here, some features can be uniquely traced from image to image. The two bright outer features labeled A and B in Images 3 through 6 (see Fig. 1) both move away from the middle one. It is clear that the SS 433 "jet engine" is in the central feature, and that there is a blob

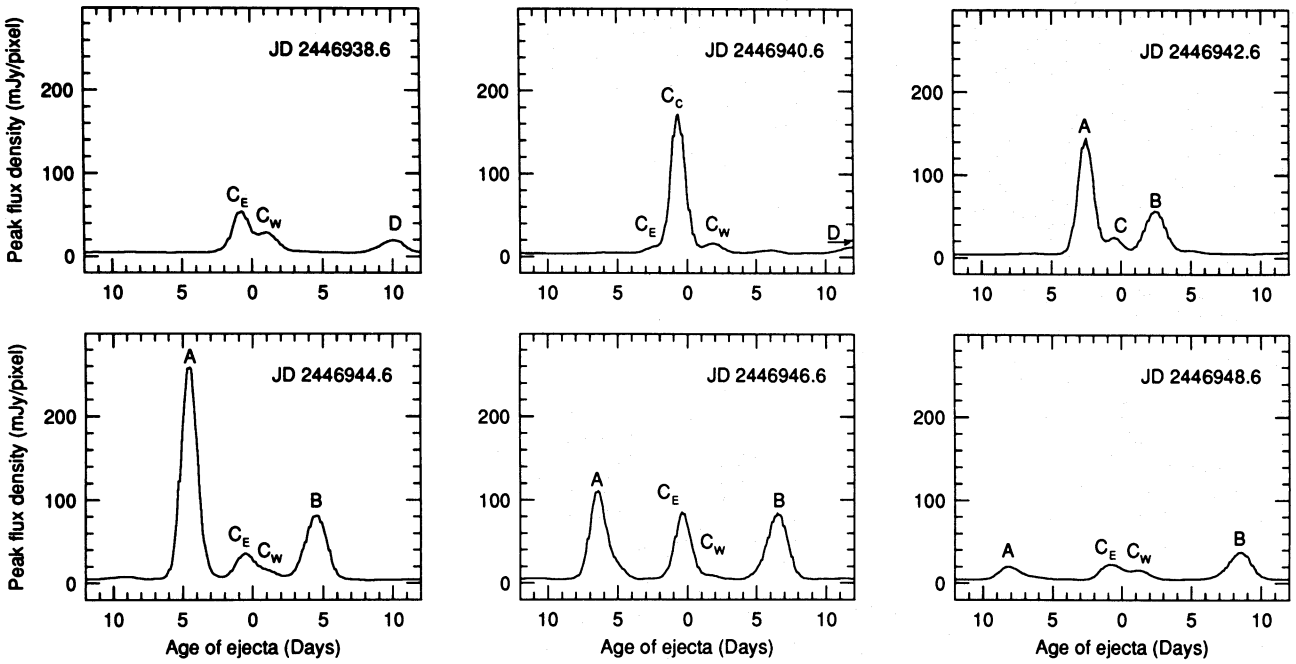

Fig. 2. Crosscuts through the images in Fig. 1 along the curved locus of emission predicted by the kinematic model. All crosscuts have been drawn at the same (arbitrary) intensity scale, to facilitate studying the evolution of individual features

in each jet. It is worthwhile to stress that the core is in fact not the brightest component in Images 3 through 6. The *relative* positioning of the images shown in Fig. 1 is accurate at about the 1 mas (5 AU) level. It is the only configuration which yields a constant (but different) proper motion for both of the prominent blobs A and B, as well as for the fainter outer blob D. The latter can be traced through the first four images, and therefore enables Images 1 and 2 to be tied in to the sequence.

3.2. The location of the core

The core component is a complex feature, with protrusions along one or both jets, spanning >100 AU. There is no clear two-sided proper motion in this core complex, which would pinpoint the exact location of the SS 433 binary system within it. The separation of the outer blobs cannot be used for a precise determination of the core position either, since their times of ejection cannot be determined with sufficient accuracy from independent observations (e.g. the total radio flux monitoring of Vermeulen et al. 1993a). However, the curved locus of the radio emission as predicted by the kinematic model can serve as a guide.

Figure 1 shows the kinematic model prediction in our adopted registration. In the figure, the distance to SS 433 was taken to be 4.9 kpc, in agreement with earlier work (e.g. Romney et al. 1987) and with the proper motion of features in our series of images (see Sect. 3.4). We have used the 5-parameter kinematic model as given by Margon & Anderson (1989), and the nodding motion as derived by Vermeulen (1989) from the radial velocity formalism of Katz et al. (1982). The validity of the parameter values at the time of the observations was confirmed by the spectroscopy of Vermeulen et al. (1993b). The position angle of the precession cone projected onto the plane of the sky is not a parameter in the optical kinematic model. It can be obtained from fits to the images; our result is consistent with earlier determinations, but has a larger error margin. In Fig. 1 we have adopted the value (100°) derived from VLA images (Hjellming & Johnston 1981b) and arc-minute scale X-ray emission (Watson et al. 1983); those datasets have more resolution elements over the full maps than our EVN images.

The emission locus in the inner jets as predicted by the kinematic model is relatively straight (see Fig. 1). From fits by eye we estimate that there is a total range of $\leq$ 10 mas (50 AU) in which the centre of the system could be placed. We reiterate that this is only one degree of freedom for the entire *series* of images, since the relative alignment is fixed by requiring constant proper motions (Sect. 3.1).

The absolute registration of the kinematic model shown in Fig. 1, i.e. our choice for the position of the core, was achieved by assuming that blobs A and B were ejected simultaneously. This implies choosing the centre such that the peaks of those two blobs lie at equal age marks on the predicted locus. Due to differential light travel time, this is *not* equivalent to their being at equal projected angular distances from the core. Our choice falls within the margin allowed by the requirement of a good overall fit to the shape of the kinematic model curve. Figures 1 and 2 show that this choice of the centre also leads to a symmetric projected extent of the core complex in most of the images. However, the flux density distribution in the core component is rather asymmetric: the peak is always to the east of the centre.

It would also be possible to choose different ejection times of the outer blobs. One could shift the kinematic model prediction

on the plane of the sky in such a way that the SS 433 binary system would coincide with the peak of the central radio feature in all six images. This choice would follow the preferred location in earlier work, but would imply that the western blob B was ejected $\sim$ 1 day earlier than the eastern blob A. It would also mean that the core complex is systematically extended further to the west than to the east.

While these two alternative registrations, and any intermediate ones, give acceptable fits between the features in the images and the kinematic model prediction, we believe the best correspondence is obtained when blobs A and B are assumed to have been ejected simultaneously, as drawn in Fig. 1. More importantly, however, for our preferred registration there is, after compensation for differential light travel-time, no persistent asymmetric source structure, which we would find difficult to explain, particularly near the core. Furthermore, the excess flux density in the eastern portion of the core, implied by our choice, can be explained naturally by Doppler favouritism, as will be discussed in Sect. 4.1.1. Finally, in our preferred registration the evolution of the knots in the VLBI images corresponds well with the integrated radio emission monitored by Vermeulen et al. (1993a). We feel that the registration shown in Fig. 1 is the only one in which the properties of both the core complex and the outer knots are readily understood in terms of the well established kinematic model. Our choice leads to an ejection time for blobs A and B of ~JD 2446940.0. Knot D was ejected at ~JD 2446928.5 in the registration of Fig. 1.

3.3. Nodding motion

Note that the nodding motion is included in the predicted locus; this has not been done in previous radio work. It results in a displacement on the sky which increases with distance from the centre; the effect is most noticeable in the bright outer portions of the jets. In particular, the fainter tail-like portion of knot A in the last three images does not point back in a straight line to the core, but follows the wiggles predicted by the nodding motion. This is the first time that non-Doppler evidence for nodding motion has been revealed. We have also verified for the maps presented in Paper I that, while not required by the data, inclusion of nodding motion leads to an improved fit.

3.4. Distance and velocity determination

The size-scale of the curved ejection pattern in an individual radio image yields an estimate of the (angular) proper motion. Hence, with the absolute (linear) value of the motion, one can obtain the distance to SS 433. Some published values are 5.0 ± 0.3 kpc (Fejes 1986b) and 5.0 ± 0.5 kpc (Romney et al. 1987). These numbers are based on the velocity derived from optical work (0.260 c). Light travel-time differences between the approaching and receding side lead to asymmetry between the two curved traces, and in principle this allows a determination of both the speed and the distance from radio data alone. Hjellming & Johnston (1981b) found 0.26 ± 0.05 c and 5.5 ± 1.1 kpc, using a pair of knots in VLA images which were assumed to have been ejected simultaneously.

A more direct approach is to follow the proper motion of individual blobs in the jets of SS 433. This was done for MERLIN images by Spencer (1984); the distance was found to be 4.9 ± 0.2 kpc. The success of such attempts hinges on the proper identification of moving entities in different images. We wish to draw attention to the fact that in VLA images which encompass more than one precession cycle, projection effects may well lead to local brightness enhancements; see for instance the images published by Hjellming & Johnston (1985). The apparent movement of such features, as opposed to the actual bulk motion in the jets of SS 433, may introduce errors. Our EVN images span only a small fraction of the precession cycle.

In determining proper motions from the images, some uncertainty is introduced by the broadness of, in particular, the eastern blob. The brightest parts of A and B separate *from each other* at a constant rate; those peaks were therefore used for the velocity estimates. The western blob (B) separates *from the core* more slowly that the eastern one (A). Thus, a direct comparison of the proper motion of two uniquely identifiable blobs with respect to the core, confirms that the western jet in SS 433 recedes from us (at this phase of the precession cycle). This result was already inferred from the curvature seen in many previous images at various resolutions (e.g. Hjellming & Johnston 1981b).

Since the inner kinematic model trace is relatively straight, there is a range of separate ejection times for blobs A and B which yield acceptable fits to the evolving morphology (see Sect. 3.2). In view of the rapid nodding motion, the two blobs therefore do not necessarily move in anti-parallel directions. By fitting separate projected velocities to the measured peak positions for A and B (each estimated to be accurate to ± 2 mas), and then assuming a single intrinsic jet velocity, we find that this velocity is 0.255 ± 0.015 c, and the distance to SS 433 4.80 ± 0.35 kpc. Both values are consistent with earlier work, but clearly, optical spectroscopy allows a more accurate velocity determination (e.g. Margon & Anderson 1989). As discussed in Sect. 3.2, it is plausible that blobs A and B were ejected simultaneously (in anti-parallel directions); in that case, they would move at 63° to the line of sight. Using this ejection angle, and adopting the optically determined velocity of 0.260 c, thus constraining the proper motion of peaks A and B to be different only due to light travel time, we find a distance to SS 433 of 4.85 ± 0.2 kpc.

3.5. Compact structure; transatlantic baselines

Green Bank joined the EVN on Days 1, 5, and 6. On the transatlantic baselines, no believable 6σ fringes were detected at all for SS 433 on Day 1, and only very few on Day 6. All calibrator scans yielded detections, so a technical failure seems unlikely. Clearly, on Days 1 and 6, SS 433 was almost completely resolved between the EVN and Green Bank; most of the emission at 5 GHz originated on size scales larger than $\sim$ 2 mas. A very conservative estimate is that on Days 1 and 6 no $\leq$ 1.3 mas

($\leq 10^{13}$ m) features exceeded a flux density of 50 mJy. This agrees with the results of earlier work at other frequencies by Walker et al. (1981) and Geldzahler et al. (1981).

Fringe amplitudes could be determined for most of the scans on Day 5, when the total flux density of SS 433 was significantly higher. However, we were unable to recover phase information at the high spatial frequencies using closure-phase constraints, since Green Bank was such an outlying station in our network. The visibility amplitudes on Day 5 can be fitted satisfactorily with models consisting of two 1–2 mas FWHM gaussian components, separated by $\sim$ 60 mas along a line in a position angle of $\sim$ 117°. This distance and position angle suggest that one compact component is located in the core, and the other in blob A.

Simultaneous model fitting of the EVN and the transatlantic visibilities on Day 5, using several gaussian components with a FWHM of $\sim$ 10 mas, in addition to the two 1–2 mas FWHM features, did not produce consistent results. This may be due to the large hole in the (u, v)-plane coverage, but on the other hand such a rigid separation of scales is probably not very appropriate for the features in the jets of SS 433. Consequently, it is difficult to determine the total flux density in compact structure. Using a fixed FWHM of 1.3 mas ($\sim 10^{13}$ m) for the two compact features on Day 5, we find that one knot contains $\sim$ 55 mJy and the other $\sim$ 25 mJy. There is insufficient data to constrain possible additional weak ($\sim$ 10 mJy) compact components, either in blob B, or as substructure within one of the major features of the EVN images (e.g. the core complex).

3.6. Description of the evolving structure

In the kinematic model analysis presented above, we have distinguished emission in the jets at some distance from the centre, and emission originating in a complex core component. We have drawn attention to the uncertainty in locating the binary system within that central component. The features in Figs. 1 and 2 are labeled with different letters. Table 2 lists their integrated flux density, measured from the images. "C" designates the entire core complex, and "C_E", "C_C" and "C_W" are used for the eastern, central, and western parts, wherever such a division appears appropriate.

Table 2. Integrated flux densities (mJy) of distinct features, measured from the images. Labels A to D are shown in Figs. 1 and 2

Image	Core				Knot A	Knot B	Knot D
	C_E	C_C	C_W	Total			
1	63		27	90			15
2	5	175	10	190			6.5
3		22		22	151	57	5
4	32		9	41	287	83	2.5
5				90	149	89	
6	25		11	36	25	41	

Image 1 displays an elongated central component, in which a brighter C_E and a weaker C_W can be distinguished. If the binary system lies on the brighter peak, the western protrusion extends twice as far as the eastern one. Our preferred registration yields a more symmetric structure, but with an unequal flux density distribution. There is also an outlying component D in the western jet.

Knot D has faded in Image 2, whereas the core complex has then become very much brighter. It appears to consist of three parts, and although it is slightly more extended than in Image 1, the rate of expansion is at most one third of that expected in the kinematic model as the result of motion in the jets. In our preferred registration, the complex is still roughly symmetric in extent, but asymmetric in flux density.

Image 3 shows the birth of the bright pair of blobs A and B. Blob A dominates the total flux density distribution. Since A and B are quite close to the centre, one cannot distinguish substructure in the core. If more or less permanent extensions to the core exist, they would make (relatively minor) contributions to the total flux densities of A and B listed in Table 2. Knot D is still present and fading. We stress that according to the kinematic model, peaks C_E and C_W in Image 2 do not correspond to blobs A and B of Image 3, which are in nearly the same location. However, a possible connection of the peak of C_W in Image 2 and the faint western extension to knot B in Image 3 cannot be ruled out.

Blobs A and B have moved outward in Image 4, to reveal a core which looks quite similar to that in Image 1: a brighter eastern portion, and a weaker western section. Blobs A and B have both brightened, while D is now just visible above the noise. Knot A is extended along the jet direction, but is unresolved perpendicular to the model trace. A bridge of faint emission links components A and B to the core complex. There is no trace of the western tip of knot B which was visible in Image 3.

By Image 5, knot A has faded, while knot B is still increasing in total flux density. Knot D could no longer be found above the noise level (1.5 mJy/beam). Both bright blobs are now clearly separated from the core by a region without emission at the achieved 100:1 signal-to-noise ratio. Both blobs are elongated along the jet direction, as is the core. The core is now brighter than in Images 3 and 4; its structure is again compatible with a brighter eastern wing and a weaker western one.

In Image 6, finally, all components have faded. Both A and B are extended along the jets; their brightest parts show a constant proper motion. The knots are widely separated from the core. The shape of the core is strikingly similar to that in Image 1.

4. Discussion

The set of six EVN images displays many of the features discussed in Paper I and also seen in earlier maps (e.g. Romney et al. 1987). We now believe that a typical VLBI image of SS 433 at 5 GHz displays a core component, which is extended along the jets, and additional individual evolving features (blobs) at larger distances in both jets. All components have variable flux

densities. Blobs in the jets brighten while moving out to 200–300 AU, and fade thereafter. We will now discuss the properties of the core complex and the brightening zone in turn, and we then comment on the connection between the observed flux density evolution of these components and the radio flares observed by Vermeulen et al. (1993a).

4.1. The core complex

All of the images show good evidence for extensions of the core along both jets. They are best seen in Images 1, 4, and 6. In Image 3 they are hard to recognise due to the proximity of blobs A and B. Flaring confuses the central region in Images 2 and 5; the structure is consistent with a central feature with two wings.

4.1.1. Symmetry and Doppler boosting

In our preferred registration the angular extent on the sky is similar for the two wings. Note that an equal angular extent can result both for radio emission from nearly stationary matter and for emission from matter moving with relativistic speeds, as long as the brightness profile is the same along both jets in their own co-moving reference frame, i.e. as long as there are no intrinsic differences between the two jets. In the case of bulk relativistic motion, however, one observes matter ejected over a longer timespan in the receding jet than in the approaching one.

The emission is brighter on the eastern side. In Images 1 and 6, where the division into C_E and C_W is clearest, the brightness ratio is ~ 2.3 (see Table 2). The well-known Doppler boosting formula for continuous jets (e.g. Fejes 1986a) predicts a ratio of 1.7 between intrinsically equally bright jets with velocity 0.26 c, if they are at $\sim 67°$ to the line of sight (typical for the jets near the core during the observations), and have a spectral index of -0.6 ($S \propto \nu^{\alpha}$). The predicted ratio becomes 1.5 for $\alpha = 0$. For a comparison between individual blobs rather than continuous jets, a ratio of 2.1 would be applicable (with $\alpha = -0.6$). The measured brightness ratio is rather sensitive to the exact location of the centre in the images. There may be an unknown contribution from radiation which originates in the vicinity of the SS 433 binary system, and, of course, the intrinsic flux density need not be exactly the same in the two jets. Given these uncertainties, we believe that the observed east-west flux density asymmetry of the core wings can be explained quite well by the expected Doppler boosting of matter moving at 0.26 c.

Similar wings near the centre were noted in Paper I, and, again, there is evidence for these features in all 6-cm data presented by Romney et al. (1987). Yet another instance of the same phenomenon occurs in the series of maps from rather limited arrays analysed by Schilizzi et al. (1984). These authors discussed a "blowpipe", thought to be an elongated cavity in which the energy of a radio flare would be transported by particles moving at 0.26 c, until a discrete blob would form at its tip.

The maps in Paper I and the May and June 1981 maps in Romney et al. (1987) do not show much flux asymmetry near the centre. The jets of SS 433 were closer to the plane of the sky in those maps, and hence differential Doppler boosting is expected to be insignificant. We also remark that Schilizzi et al. (1984) found rather asymmetric structures with a higher flux density in the eastern jet, at a time when significant Doppler favouritism would indeed be expected. The April 1981 map in Romney et al. (1987) could be a counter-example: the jets were close to the plane of the sky, yet the eastern feature close to the core was brighter than its western counterpart. Note, however, that the features in that map do not have a continuous appearance, and hence they are perhaps not akin to the core wings presently under discussion. Rather, they may resemble "blobs", such as A and B in our images, which are usually seen at greater distances, and in fact, they could be analogous to the more discrete features seen in the first map of Paper I. It was suggested in Paper I that transient flux density differences between such blobs may occur.

We conclude that the east-west flux density asymmetry of the core components in the images strongly suggests that the radio emission originates in matter which is actually moving at 0.26 c in the jets, rather than in a cocoon of disturbed (circumstellar ?) matter which is stationary or moving only slowly. The present observations therefore do not support the existence of a blowpipe as suggested by Schilizzi et al. (1984).

4.1.2. Evidence for continuous ejection

The resolution and time coverage of the EVN images do not permit us to probe travel timescales much smaller than one day or length scales much smaller than 50 AU. Since the fringe amplitude is very low on transatlantic baselines at 5 GHz (see Sect. 3.5), there is little compact structure left to be uncovered by observations at higher resolution. The fact that the core wings are present in many of the 5 GHz images obtained to date, the fact that these wings probably extend equally far along both jets (≤ 100 AU), and the strong suggestion that they are emitted by matter moving at 0.26 c, together imply that there is a quasi-continuous injection of radio emitting matter into the two jets of SS 433.

4.1.3. Brightening and fading in the core wings

The radio brightness in the core wings drops after ~ 2.5 days of travel. This is presumably due to adiabatic expansion or some other change of the magnetic field or particle configuration. It is intriguing that this fading timescale is rather comparable to that for the evolving optical emission line bullets (e.g. Vermeulen et al. 1993b), but while the expanding jet geometry could well provide an indirect connection between the optical and radio fading, the physical mechanisms responsible for the thermal and non-thermal emission are probably sufficiently dissimilar that no detailed correspondence exists between the rather discrete optical bullets and the more continuous radio core wings.

The uncertainty in locating the binary system in the VLBI images leads to a corresponding uncertainty in the derived flux density profile in the wings. In the present images, the most plausible configuration often does not have a central brightness peak (see Fig. 2). Rather, C_E and C_W appear to be separate entities, suggesting that the radio brightness of the wings is

greatest $\sim$ 30 AU from the centre. However, this idea is not supported by earlier maps (e.g. Paper I). The appearance of Images 2 and 5 suggests that, apart from the wing-like (jet) emission, there is also radiation which originates in the vicinity of the SS 433 binary system. That component is quite variable, as also witnessed by the maps in Paper I, and earlier work. This variable contribution to the core area hampers a study of the brightness profile of the wings. A more extensive series of images will be needed to address this problem. A possible connection between the appearance of blobs in the jets of SS 433 and a brightening of the central component, such as displayed by Images 2 and 5, will be discussed in Sect. 4.3.

4.2. Blob evolution in the brightening zone

4.2.1. Confirmation of the brightening zone

In Paper I, we deduced the existence of a brightening zone, located at $\sim 4 \times 10^{13}$ m (250 AU) from the binary system. The radio flux density from individual knots, moving as predicted by the kinematic model, was found to increase at that distance. In Paper I and in Fejes et al. (1988) it was pointed out that many earlier maps (e.g. Romney et al. 1987) had radio features at about the same distance, suggesting that the brightening zone is a permanent phenomenon. In the series of EVN images we present here, blobs A and B undergo substantial brightening during the first $\sim$ 5 days of their existence (see Fig. 2 and Table 2). Rapid fading sets in beyond $\sim$ 250 AU, in agreement with the evolution described in Paper I.

The permanent existence of the brightening phenomenon now seems well established, though there are differences in the detailed behaviour of particular blobs. In contrast to the maps described in Paper I, the present series is dominated by a single pair of blobs, A and B, and they are already quite bright at $\sim$100 AU from the binary system. They could be analogous to, but much brighter than, the discrete knots close to the core in map 1 of Paper I, and similar features in the April 1981 map of Romney et al. (1987). On the basis of the images presently available, we hesitate to say whether there is usually a sudden increase in brightness at 200–300 AU (the brightening zone as described in Paper I), or whether knots typically show a more gradual increase in total flux density as they move from the core out to this distance. In the latter case, it would be more appropriate to call the entire $\sim$250 AU sphere around SS 433 the brightening zone. Such a situation would remove the somewhat awkward need for a well-defined distance at which much more synchrotron radiation is suddenly produced. The brightening at 5 GHz could in that case be due to the fact that the blobs gradually expand and become optically thin.

4.2.2. Symmetry between the jets

The images are consistent with an intrinsically equally fast flux density evolution of blobs A and B: we observe a slower evolution in B due to light travel-time effects. Similarly, knot D could represent a case of one-sided ejection, but if an intrinsically equally bright partner would have been simultaneously ejected into the eastern jet, $\sim$ 10 days before Image 1 was observed, then this feature would appear in Image 1 at an age of 11.5 days, as opposed to 8.8 days for knot D. Therefore, given the rapid fading which probably occurs during that time, the eastern counterpart may already have been too faint to observe. Note also that while the different peak flux densities reached by knots A and B (see Table 2) could be intrinsic, it is suggestive that their brightness ratio comes much closer to unity when their predicted Doppler boosting ratio is taken into account (2.3, assuming ejection at 63° to the line of sight and $\alpha = -0.6$). On the basis of the present set of images and earlier work (Paper I, and Romney et al. 1987) it is likely that the two jets usually display a symmetric evolution.

4.2.3. Evidence for continuous ejection

Knots A and B are not spherical, and it may not be appropriate to model them as "cannonballs". As they move away, they broaden much more in the direction of motion than perpendicular to it. This is especially obvious in the eastern blob. Note that the brightest parts, close to the leading edge, have a constant proper motion. A "tail" seems to be developing, in analogy to the effects discussed in Paper I. It is possible that such a feature is due to relativistic electrons "left in the wake" of a moving blob due to the bow-shock geometry (see for instance Icke 1988). However, as stated in Sect. 3.3, we believe that the trailing emission follows the wiggles of the nodding motion in the images. In that case, those features indicate the brightening at a more or less fixed distance of successive new portions of matter in the jets of SS 433, as was suggested for the maps in Paper I. We cannot unambiguously distinguish closely spaced clumps of matter from a continuous flow, though the data on the longest baselines (discussed in Sect. 3.5) indicate that there is little structure on scales smaller than $\sim$ 50 AU. Note that this implies that the radio features are typically rather more extended than the optical bullets (e.g. Vermeulen et al. 1993b). We believe that the evidence favours the quasi-continuous presence of weakly radiating ejecta in the brightening zone of SS 433, in a natural extension of the quasi-continuous ejection in the core region, discussed in Sect. 4.1.2.

4.3. Flaring; brightening and fading regions

Total flux density measurements during the 1987 campaign by Vermeulen et al. (1993a) show that SS 433 underwent a transition from its radio quiet mode to the flaring state; a series of radio flares was monitored. The first flare took place between the observations of Image 2 and Image 3. The total flux density at 5 GHz then dropped before rising at the onset of flare 2, which peaked close to the time when Image 4 was observed. Vermeulen et al. (1993a) found that the spectral evolution of the two events was different. Flare 3 peaked during the observation of Image 5, and flare 4 reached its maximum well after the VLBI observations had ended.

The images unambiguously show that the first flare is connected with the bright complex core component as observed in

Image 2. The second flare, on the other hand, is related to the brightening blobs in the jets, particularly to blob A in Image 4. From a back-projection of the proper motion of knots A and B in Images 3 through 6, it would follow that the bright core feature C_C in Image 2 shows these knots at a very early stage in their evolution. However, it is important to note that the first two radio flares, as observed by Vermeulen et al. (1993a), were clearly separate events, with an intervening drop in total flux density. This indicates that the knots did not brighten steadily from their generation out to the edge of the brightening zone. The brightening of the central component in Image 2 is clearly a precursor to the appearance of knots A and B in Image 3. Hence, flares may occur in pairs, with one peak at the time when knots are ejected, and another peak ~5 days later, when these knots reach the brightening zone.

The third flare, during Image 5, was observed only as a break in the falling trend of flare 2. It is probably due in part to the brighter core complex visible in Image 5 and in part to the fact that blob B, in the receding jet, was still brightening between Images 4 and 5, and faded only between Images 5 and 6. One could postulate, in analogy with flares 1 and 2, that the core brightening in Image 5 was a precursor to the later appearance of blobs in the brightening zone, but that Image 6 was observed too early to detect these knots. It is intriguing that the predicted time of maximum brightness for such postulated knots, roughly JD 2446951.5, corresponds well with the time of the peak of flare 4 in the database of Vermeulen et al. (1993a). Speculatively, therefore, the central brightening in Image 5, partly responsible for flare 3, could form another pair with flare 4, but at a lower flux density than flares 1 and 2.

In our preferred registration of the core, the older blob D was ejected at ~JD 2446928.5 . While SS 433 was quiescent at that time, the database of Vermeulen et al. (1993a) shows that small flux density variations did occur. Unfortunately, there was no radio monitoring above 1415 MHz in the days immediately preceding the ejection of knot D. However, daily monitoring at 1415 MHz shows a small peak on JD 2446929.2. From JD 2446929 to JD 2446933 the total flux density decreased at 1415, 2695, and 8085 MHz. There was then a slow, ill-defined maximum around JD 2446934. The data are insufficient as a firm basis for an association, but it is suggestive that higher flux densities occurred at the extrapolated time of ejection of knot D, as well as at its time of passage through the brightening zone.

The maps in Paper I, which show clear blob production, were observed when SS 433 was radio quiet. Radio blob production evidently does not cease entirely during periods termed quiescent on the basis of the global total radio flux density evolution. Even small peaks in the flux density data may be indicative of the formation of radio knots. In the available radio images there is no evidence for behaviour of a truly different nature at times of flaring than at quiescent times: blobs A and B in the 1987 images show the same brightening and fading cycle as their much fainter counterparts in the 1985 set of maps. Note, however, that the images presented here show the first instance of blobs which are brighter than the assumed core.

As stated above, it is likely that the bright core C_C in Image 2 shows the two knots A and B very soon after their ejection. Given the total flux density evolution (Vermeulen et al. 1993a), these knots must then have faded. It is plausible that this is due to the same mechanism which also limits the extent of the core wings, as discussed in Sect. 4.1.3. Afterwards, the brightness of the blobs increased once more, as they progressed through the brightening zone. This scenario therefore calls for two zones of brightening and fading of material in the jets of SS 433, with maxima in flux density occurring at $\sim$ 30 AU and $\sim$ 250 AU from the centre, respectively, though we emphasise that the location of the first maximum is very uncertain. The brightening zone and the core wings can be viewed as regions in which radio emission will preferentially be produced by matter passing through. However, while there is evidence for quasi-continuous ejection, the actual amount of synchrotron radiation produced at a given time varies strongly; the configuration is far from stationary. We have argued that there is usually, if not always, radiation from the core wings, but the total flux density is variable (compare Images 1 and 2 of the present series). Furthermore, not all matter undergoes a significant second brightening. For instance, the matter which is visible in the wings of Image 1 does not "light up" significantly when it reaches the brightening zone in Image 3 or 4. In contrast, if the bright central component of Image 2 is indeed caused by the initial bright phase of blobs A and B, then these features undergo such a strong second brightening that they reach a higher flux density in the brightening zone than in the core wings. The material trailing behind blobs A and B could represent an intermediate case: it is responsible for the core wings in Image 4, and it brightens again in the "tails" of blobs A and B in Images 5 and 6.

In Paper I, it was pointed out that if the jets of SS 433 are blob-like, then in the precession geometry of SS 433 each blob will overtake the bow-shock of its predecessor at a well-defined distance, which depends only on the Mach angle of the bow-shock. Such a mechanism is not valid for continuous jets, and it may also not be a fruitful model to describe more gradual brightening. The total flux density data of Vermeulen et al. (1993a) suggest that relativistic particles are generated in a sustained process. The brightening zone may arise as the result of this ongoing relativistic particle production, probably coupled to a gradually falling optical depth due to expansion. Further adiabatic expansion would then lead to fading, as was already suggested in Paper I. It was also pointed out in that work that beyond $\sim$ 250 AU the jets of SS 433 enter a zone which has probably not yet been filled in by the stellar wind since the last passage of the jets one precession cycle earlier. Hence, this is a likely distance at which sudden expansion may occur. The detailed physical conditions in the jets of SS 433 remain unclear. Magnetic field variations and changes in the relativistic particle population, possibly due to shocks, will need to be considered together with the effects of (adiabatic) expansion of the bulk flow. This issue will be explored more fully in a future paper that will combine the present series of images with the radio monitoring data presented in Vermeulen et al. (1993a).

5. Summary

We have discussed a series of six high dynamic range VLBI images, with a resolution of 10 mas. It is remarkable how closely the radio emission traces the bulk flow at 0.26 c described by the kinematic model. We have shown that the evolution seen is consistent in all respects with the kinematic model parameters derived from many years of optical measurements. A distance to SS 433 of 4.85 ± 0.2 kpc fits the data best. This work for the first time reveals the presence in radio images of the six-day nodding motion. We have found evidence for Doppler boosting, indicative of matter moving at 0.26 c, both in emission from individual knots in the jets of SS 433, and in more continuous emission closer to the binary system.

We believe most of the structure revealed by this series of radio images is intrinsically symmetric. In the light of all previous maps, we conclude that symmetric ejection of material in the two jets of SS 433 seems to be the rule. The detailed evolution of the radio emission is not identical in both jets; local effects as well as Doppler favouritism may contribute to the occasionally asymmetric structures.

The images strongly support the existence of the brightening zone. Radio knots become brighter at 5 GHz while they travel out to $\sim$ 250 AU, and they fade rapidly thereafter. Tail-like features in the later images are probably due to new portions of the jets which enter the brightening zone.

The core region is quite complex, and has wing-like extensions, each spanning $\sim$100 AU. We have shown that earlier VLBI maps are consistent with the permanent presence of these wings. Possibly, the material responsible for the wings reaches its maximum brightness at some distance from the centre ($\sim$ 30 AU ?). Probably, a substantial fraction of the radio emission from the complex core region originates in quasi-continuously ejected matter during the first two days of travel in the jets of SS 433, because the observed flux density ratio between the two sides indicates motion at 0.26 c, while these wings appear to be stationary features in the images.

Transatlantic VLBI shows that most of the 5 GHz emission is distributed on scales larger than $\sim$ 10 AU. This is further evidence that the radio emitting material is ejected quasi-continuously; as stated above, the properties of the core wings and the brightening zone support this.

We have established that radio flares may occur both in the core-plus-wing region, and in the brightening zone. We have found at least one instance, and possibly more, where a flare in the core component was related to the subsequent emergence of bright blobs in the jets. In many cases more than one region is involved in a flare, if only because there is a blob in both of the jets. Given that the production interval for discrete VLBI knots and the fading timescale of such knots both seem to be of the order of a few days, such events will frequently overlap and mask each other in the radio spectrum of SS 433. Therefore, it is difficult to study the jets of SS 433 based on the evolution of the radio spectrum without the benefit of an image.

SS 433 offers unique possibilities to study a near-relativistic jet system in closeup. We have discussed evidence for both quasi-continuous and clumped ejection in the jets of SS 433. Further imaging efforts are needed to confirm our speculative scenario which calls for a double cycle of brightening and fading, and for a quasi-continuous ejection of radio emitting matter which is intermittently enhanced. More headway in unravelling the nature of the different radio emitting features will come from VLBI spectral index images. That in turn will be a first step in charting the energy and magnetic field distribution, which may soon become feasible with sensitive VLBI polarimetry.

Acknowledgements. We thank the staff members at the five EVN observatories, and at Green Bank, who helped to assure highly successful observations. We are grateful to the staff at the Max-Planck-Institut für Radioastronomie for their advice and assistance during a smooth and speedy correlation of all the data. M. Rugers and L. Smiers are thanked for their assistance in correlating the data and producing the images, and T. Muxlow and R. Nelson for introducing one of us (RCV) to OLAF, and for their help in producing the images with this system. We thank the anonymous referee for some useful comments. RCV acknowledges support from the Netherlands Foundation for the Advancement of Research (NWO) through project 782-373-030.

References

Abell G.O., Margon B.H., 1979, Nat 279, 701
Aslanov A.A., Cherepashchuk A.M., Goranskij V.P., Rakhimov V.Yu., Vermeulen R.C., 1993, A&A this issue
Downes A.J.B., Pauls S.T., Salter C.J., 1981, A&A 103, 277
Fejes I., 1986a, A&A 166, L23
Fejes I., 1986b, A&A 168, 69
Fejes I., Schilizzi R.T., Vermeulen R.C., 1988, A&A 189, 124
Geldzahler B.J., Downes A.J.B., Shaffer D.B., 1981, A&A 98, 205
Hjellming R.M., Johnston K.J., 1981a, Nat 290, 100
Hjellming R.M., Johnston K.J., 1981b, ApJ 246, L141
Hjellming R.M., Johnston K.J., 1985, in: Radio Stars, eds. R.M. Hjellming, D.M. Gibson, Reidel, p. 309
Hjellming R.M., Johnston K.J., 1988, ApJ 328, 600
Icke V., 1988, in: The Use of Supercomputers in Observational Astronomy, ed. T.J. Cornwell, NRAO Workshop No. 15, p. 19
Katz J.I., Anderson S.F., Margon B., Grandi S., 1982, ApJ 260, 780
Kawai N., Matsuoka M., Pan H.C., Stewart G.C., 1989, PASJ 41, 491
Margon B., 1984, ARA&A 22, 507
Margon B., Anderson S.F., 1989, ApJ 347, 448
Milgrom M., 1979, A&A 76, L3
Rogers A.E.E., Cappallo R.J., Hinteregger H.F., Levine J.I., Nesman E.F., Webber J.C., Whitney A.R., Clark T.A., Ma C., Ryan J., Corey B.E., Counselman C.C., Herring T.A., Shapiro I.I., Knight C.A., Shaffer D.B., Vandenberg N.R., Lacasse R., Mauzy R., Rayhrer B., Schupler B.R., Pigg J.C., 1983, Sci 219, 51
Romney J.D., Schilizzi R.T., Fejes I., Spencer R.E., 1987, ApJ 321, 822
Schilizzi R.T., Romney J.D., Spencer R.E., 1984, in: VLBI and Compact Radio Sources, Proc. IAU Symp. 110, eds. R. Fanti, K.I. Kellermann, G. Setti, Reidel, p. 289
Spencer R.E., 1984, MNRAS 209, 869
Vermeulen R.C., 1989, Ph.D. Thesis, University of Leiden, The Netherlands, p. 9
Vermeulen R.C., Schilizzi R.T., Icke V., Fejes I., Spencer R.E., 1987, Nat 328, 309 (Paper I)

Vermeulen R.C., McAdam W.B., Trushkin S.A., Bonsignori-Facondi S.R., Fiedler R.L., Johnston K.J., Hjellming R.M., Corbin J., 1993a, A&A this issue

Vermeulen R.C., Murdin P.G., van den Heuvel E.P.J., Fabrika S.N., Wagner R.M., Margon B., Hutchings J.B., Schilizzi R.T., van Kerkwijk M., van den Hoek L.B., Ott E., Angebault L.P., Miley G.K., D'Odorico S., Borisov N., 1993b, A&A this issue

Walker R.C., Readhead A.C.S., Seielstad G.A., Preston R.A., Niell A.E., Resch G.M., Crane P.C., Shaffer D.B., Geldzahler B.J., Neff S.G., Shapiro I.I., Jauncey D.L., Nicolson G.D., 1981, ApJ 243, 589

Watson M.G., Willingale R., Grindlay J.E., Seward F.D., 1983, ApJ 273, 688

This article was processed by the author using Springer-Verlag TEX A&A macro package 1992.